CAPABILITIES FOR MAGNUS PREDICTION IN SUBSONIC AND TRANSONIC FLIGHT

J. DeSpirito* and S. I. Silton
U.S. Army RDECOM, Army Research Laboratory
Aberdeen Proving Ground, Maryland 21005-5069

ABSTRACT

The Magnus characteristics of three spin-stabilized projectiles were characterized using steady-state RANS and time-accurate RANS/LES computational fluid dynamic simulations. RANS/LES simulations improved the Magnus moment prediction for projectiles with rounded or chamfered bases. No difference was found between the RANS and RANS/LES simulations for the projectile with a sharp-cornered base—either with or without a boattail. The near-body flow field was similar for RANS and RANS/LES simulations; but the RANS/LES simulations resolved the turbulent eddies in the projectile wake. Magnus moment effects were found to be confined to the rear end of the projectile. The effects of projectile base shape on Magnus were characterized, demonstrating that boattail and hemispherical base configurations have the largest effect on Magnus moment.

1. INTRODUCTION

The capability to accurately predict dynamic aeroballistic coefficients (i.e., roll-damping, pitch-damping, and Magnus moments) via computational fluid dynamic (CFD) simulations has advanced in recent years as improved computational resources and solver technologies have become available. Accurate prediction of the dynamic coefficients is critical for the determination of the stability characteristics of projectiles and is even more important with the advent of smart, precision munitions. The roll-damping moment has been predicted with reasonable accuracy for many years in conjunction with the prediction of the static aerodynamic coefficients using steady-state CFD simulations. While a steady-state method was proposed for the prediction of pitch damping of both spin- and fin-stabilized projectiles in the 1990s (Weinacht et al., 1997; Weinacht and Sturek, 1990), that method and several time-accurate methods are just recently being applied (DeSpirito et al., 2008).

The prediction of the Magnus moment in the supersonic and high-transonic flight range was demonstrated in the 1980's (Sturek and Schiff, 1982; Nietubicz et al., 1983; Sahu, 1991). Recent work (Weinacht, 2007), directly comparing time-accurate and steady-state methods to predict the Magnus moment in the supersonic regime, showed each method accurate to within the experimental data. However, the authors recently found that the standard steady-state CFD predictions of the Magnus moment of the 25-mm M910 training and standard 0.50-cal. projectiles diverge from the experimental data as the Mach number approaches 1.0 and below (Silton, 2005; DeSpirito and Heavey, 2004). Furthermore, the use of time-accurate, hybrid Reynolds-averaged Navier-Stokes (RANS)/Large-Eddy Simulation (LES) calculations more accurately predicted the Magnus moment in the subsonic and transonic ranges (DeSpirito and Heavey, 2004). Additional computational studies were undertaken to investigate the issue on these projectiles (DeSpirito and Plostins, 2007; Silton, 2009), as well as on the U.S. Army-Navy Spinner Rocket (ANSR) (DeSpirito, 2008a).

Nonlinear Magnus moments are routinely observed for nearly all spin-stabilized projectiles at subsonic and transonic speeds (McCoy, 1998). It is important to accurately predict the Magnus moment in this Mach number range because these are the downrange velocities where trim angles often present themselves. Understanding the flight characteristics in the subsonic and transonic flight regimes is also required for direct-fire projectiles that normally operate in the supersonic regime because of training missions on range-limited proving grounds. Observing the distribution of Magnus moment along the length of a typical spin-stabilized projectile shows the nonlinearity is confined to very near the projectile base. The shape of the projectile base has a large effect on the nonlinear Magnus component (Weinacht, 2007); a rounded base was shown to exhibit a large variation with angle of attack, α, while a sharp-cornered base nearly eliminated the nonlinear Magnus effect.

The Magnus issue is related to base flow phenomena, which is an ongoing research area. In the M910 study (DeSpirito and Heavey, 2004; DeSpirito and Plostins, 2007), significant differences in the near-body wake of the projectile were observed between steady-state RANS and time-accurate RANS/LES simulations at subsonic and transonic speeds. It was speculated that the unsteady base flow interacts with the asymmetric pressure distribution (which is responsible for the Magnus effect) on the projectile body. Some or all of this interaction effect is not captured by the steady-state simulations. The wake effects on the body forces are likely small enough not to significantly impact the normal force and pitching moment; however, the Magnus force is much smaller and the small wake effect perturbations can significantly effect the Magnus moment.

Other researchers have recently used time-accurate RANS/LES methods to investigate projectile base flows

Report Documentation Page

Form Approved
OMB No. 0704-0188

1. REPORT DATE	2. REPORT TYPE	3. DATES COVERED
DEC 2008	**N/A**	**-**

4. TITLE AND SUBTITLE	5a. CONTRACT NUMBER
Capabilities For Magnus Prediction In Subsonic And Transonic Flight	5b. GRANT NUMBER
	5c. PROGRAM ELEMENT NUMBER
6. AUTHOR(S)	5d. PROJECT NUMBER
	5e. TASK NUMBER
	5f. WORK UNIT NUMBER
7. PERFORMING ORGANIZATION NAME(S) AND ADDRESS(ES) **U.S. Army RDECOM, Army Research Laboratory Aberdeen Proving Ground, Maryland 21005-5069**	8. PERFORMING ORGANIZATION REPORT NUMBER
9. SPONSORING/MONITORING AGENCY NAME(S) AND ADDRESS(ES)	10. SPONSOR/MONITOR'S ACRONYM(S)
	11. SPONSOR/MONITOR'S REPORT NUMBER(S)

12. DISTRIBUTION/AVAILABILITY STATEMENT
Approved for public release, distribution unlimited

13. SUPPLEMENTARY NOTES
See also ADM002187. Proceedings of the Army Science Conference (26th) Held in Orlando, Florida on 1-4 December 2008, The original document contains color images.

14. ABSTRACT

15. SUBJECT TERMS

16. SECURITY CLASSIFICATION OF:			17. LIMITATION OF ABSTRACT	18. NUMBER OF PAGES	19a. NAME OF RESPONSIBLE PERSON
a. REPORT	b. ABSTRACT	c. THIS PAGE			
unclassified	**unclassified**	**unclassified**	**UU**	**8**	

in the supersonic (Simon et al., 2006), subsonic, and transonic regimes without (Simon et al., 2007a) and with (Simon et al., 2007b) spin. Their work primarily concentrates on the demonstration and validation of their RANS/LES technique and illustrates the unsteady quantities that can be obtained with the hybrid RANS/LES methods and is limited to zero degrees angle of attack. No published work investigating non-zero angles of attack has been found, so no Magnus effects have been reported.

The use of time-accurate RANS/LES methods to compute projectile aerodynamics is a relatively new approach. Although computationally more expensive than traditional RANS approaches, RANS/LES is likely the only computationally efficient way to predict aerodynamic coefficients that are impacted by highly separated flow phenomena, such as Magnus effects and high angle of attack flight scenarios.

This paper summarizes the results of three investigations (DeSpirito and Plostins, 2007; Silton, 2009; DeSpirito, 2008a) comparing the Magnus moment predicted via standard steady-state RANS simulations with those predicted from time-accurate RANS/LES simulations. Recent results from a study investigating the effects of base shape on the projectile aerodynamics (DeSpirito, 2008b) are also presented. The original references for each work should be consulted for additional information since space limitations of this paper precluded inclusion of some details.

2. APPROACH

Three projectile configurations (Figure 1) are summarized: the 25-mm M910 training round, a standard 0.50-cal. projectile, and the 7-cal. ANSR. The M910 model is a 16.2 mm (1 cal.) sub-projectile that is 4.69-cal. long. It has a 2.54-cal. conical ogive, a 0.12-cal. chamfer at the base, and the center of gravity (c.g.) is located 3.08 cal. from the nose. The unstructured mesh for the RANS simulations consisted of 2 M hexahedral (hex) cells; while the meshes for the RANS/LES simulations consisted of 5.4 M hex cells for the supersonic simulations and 6 M hex cells for the subsonic simulations (DeSpirito and Plostins, 2007).

The 0.50-cal. projectile (1 cal. = 12.95 mm) is 4.46 cal. long, with a 0.16 cal. long by 0.02 cal. deep groove, and a 9° filleted boattail. The c.g. is located 2.68 cal. from the projectile nose. One mesh, consisting of 7.5 M unstructured hex cells was used for both the RANS and RANS/LES simulations in the most recent 0.50-cal. investigation (Silton, 2009).

The 7-cal. ANSR model has a 2-cal. (1 cal. = 20 mm) secant ogive followed by a 5-cal., cylindrical afterbody. Three c.g. locations were investigated: 3.250, 4.036, and 4.818 cal. from the nose, corresponding to those in the original experiments. The unstructured meshes for the RANS and RANS/LES simulations consisted of 5.9 M and 11.3 M hexahedral cells, respectively (DeSpirito, 2008a).

For the M910 and 7-cal. ANSR models, the meshes for the RANS/LES simulations differed from the RANS meshes primarily in the projectile wake region. In the wake region, an LES mesh (nearly isotropic cells) extended for at least 0.75–1.0 cal. rearward of the projectile base. The projectile spin rate was determined from the muzzle exit twist rate of the gun used to launch the projectile.

The commercially available CFD++ code, from Metacomp Technologies, Inc., was used. The steady-state simulations were performed with either the three-equation k-ε-R turbulence model (keR), or the cubic k-ε (cke) model, where k is the turbulence kinetic energy, ε is its dissipation rate, and R is the undamped eddy viscosity. The RANS/LES methodology of CFD++ is based on the solution of transport equations for the unresolved turbulence kinetic energy and its dissipation rate and incorporates anisotropy and low Reynolds number damping effects in both LES and RANS modes. CFD++ reverts to a cubic k-ε model on RANS-type meshes and blends automatically to an anisotropic form of the Smagorinsky model in regions of uniformly-refined mesh.

In all three projectile configurations, the near-wall mesh was designed for a y^+ of 0.5 and the far-field computational domain boundaries were set at appropriate distances for the Mach numbers under investigation. The projectile wall boundary condition was set as a rotating, no-slip wall to simulate the projectile spin. The outer boundaries were set as far-field, with a pressure of 101.3 kPa and a temperature of 288 K (M910 and ANSR) or 292 K (0.50-cal. projectile).

Simulations were performed on the Linux Networx clusters at the U.S. Army Research Laboratory (ARL)

(a) (b) (c)

Figure 1. (a) M910 projectile, (b) 0.50-cal. projectile, and (c) ANSR.

Major Shared Resource Center (MSRC). The number of processors used for steady-state runs was such that 125,000–150,000 cells were partitioned on each processor. The basic RANS calculations were run using the double-precision solver until steady state was achieved. The calculations took approximately 11–15 s of CPU time per iteration and convergence was achieved in about 600–800 iterations. The aerodynamic coefficients were the determining factor in convergence in all cases. The time-accurate RANS/LES simulations were usually performed at 2 angles of attack: α = 2° or 3° and α = 5°, and at several Mach numbers investigated in the steady-state cases. Time steps were determined based on having about 70 time steps within the period of the oscillations in the wake flow, assuming a Strouhal number of 0.25. Time steps for the RANS/LES simulations ranged from 0.8 to 4.0 μs. The simulations were run for a total non-dimensional time of 60–175. Shorter times were needed for supersonic cases, which had a shorter transition period from the steady-state solution.

For each of the three projectile configurations the static aerodynamics (i.e., axial force, normal force, and pitching moment) and roll damping were predicted accurately using steady-state RANS simulations (DeSpirito and Plostins, 2007; Silton, 2009; DeSpirito, 2008a). These simulations use a rotating wall boundary condition to mimic the spinning projectile. Individual simulations at several angles of attack are run for each Mach number. In addition, accurate predictions of roll damping are obtained from these simulations. Magnus moment predictions are also obtained from these steady-state RANS simulations and were generally found to be accurate in the supersonic flight range. However, at lower Mach numbers, the Magnus moment predictions were usually less accurate, with the magnitude of the difference depending on projectile shape. Reasonably accurate pitch damping—to within the experimental error—is obtained from a separate steady-state simulation that uses a rotating reference frame to model the projectile under a coning motion (Weinacht et al., 1997; DeSpirito et al., 2008). This simulation procedure is called the "virtual wind tunnel" approach (Weinacht, 2007) because it resembles the experimental procedure used in wind tunnel testing.

3. RESULTS AND DISCUSSION

The investigation of the M910 projectile was the first to find that time-accurate RANS/LES simulations could provide more accurate Magnus moment predictions (DeSpirito and Heavey, 2004; DeSpirito and Plostins, 2007). The Magnus moments of the M910 at α=3° and α=5° are shown in Figure 2. The steady-state RANS simulations show only a small decrease in value as the Mach number decreases through the transonic and

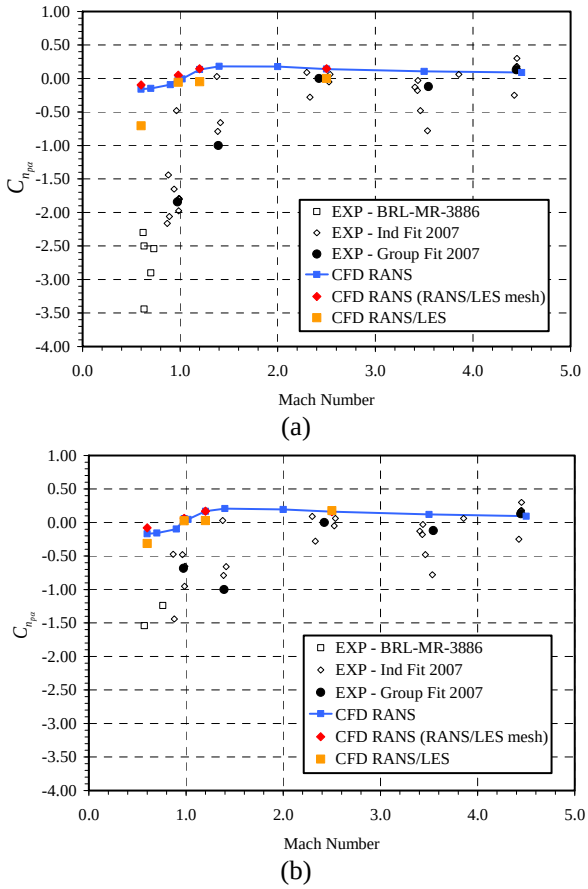

Figure 2. Comparison of predicted and experimental Magnus Moment at (a) α = 3° and (b) α = 5° for M910 projectile.

subsonic ranges. The experimental data (Plostins et al., 1991) show a more substantial decrease. The RANS/LES simulations more accurately predict the decreasing trend of Magnus moment with lower Mach numbers. In addition, the RANS/LES simulations also predict the nonlinearity with α that is observed in the experimental data at the lower Mach numbers (e.g., larger negative Magnus moments at α=3° than at α=5°). Very little nonlinearity in Magnus moment with α was predicted in the RANS simulations.

The comparison of the experimental and predicted Magnus moment for the 0.50-cal. projectile is shown in Figure 3. At α = 5°, the data trends in the RANS solution and experimental data appear to agree rather well. The agreement of the CFD prediction with the experimental data in the supersonic regime is quite good, accurately predicting both trend and magnitude. The CFD accurately predicted the critical behavior in the transonic regime. However, as Mach 1 is approached, the CFD appears to under predict the Magnus moment. The CFD again over predicts the Magnus moment in the subsonic regime. At α = 2° (Figure 3a), the RANS correctly predicts the same trend as the experimental data but the

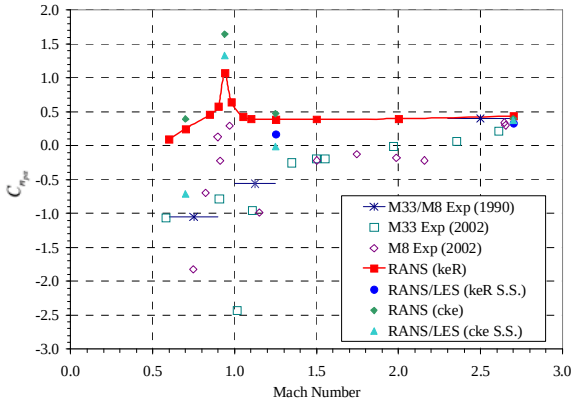

(a)

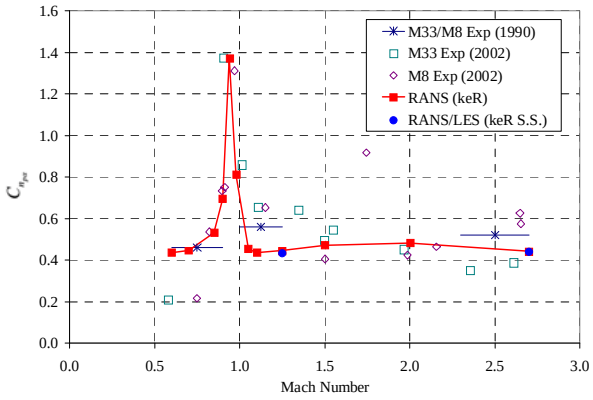

(b)

Figure 3. Comparison of predicted and experimental Magnus Moment at (a) $\alpha = 2°$ and (b) $\alpha = 5°$ for 0.50-cal. projectile.

values are over predicted for $M < 2.5$. While varying the RANS turbulence model did have a small effect on the magnitude of the Magnus moment; there was no improvement in the predictions at the lower Mach numbers. Switching to the time-accurate RANS/LES simulation–regardless of the RANS model used to start the simulation–appears to more accurately predict both the trend and the magnitude of the Magnus moment. This result is similar to that observed for the M910 projectile and, in fact, the match with the experimental data is even better for the 0.50-cal. projectile. The 0.50-cal. investigation had not been completed at the time of the writing of this paper. Additional RANS/LES simulations (Silton, 2009) will be run to better determine the shape of the Magnus moment–Mach number curve.

Figure 4 illustrates the difference in predicting the nonlinearity of the Magnus moment with α. The RANS predictions show no nonlinearity with α until the Mach number decreases below 0.85. The RANS/LES shows that the nonlinearity with α begins above Mach 1. The additional RANS/LES simulations to be completed (Silton, 2009) will further quantify the Mach number at which this nonlinearity begins.

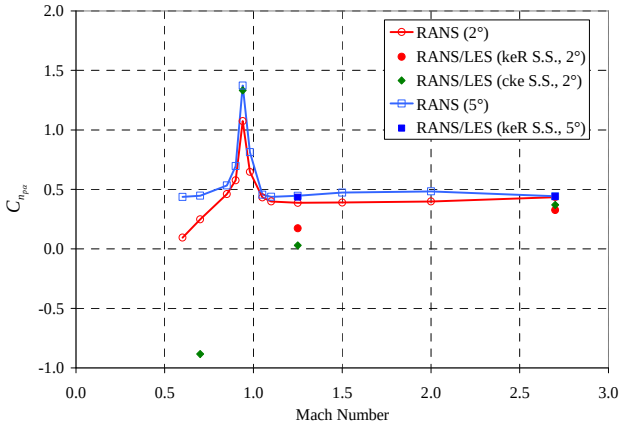

Figure 4. Comparison of predicted Magnus moment at $\alpha = 2°$ and $\alpha = 5°$ for 0.50-cal. projectile.

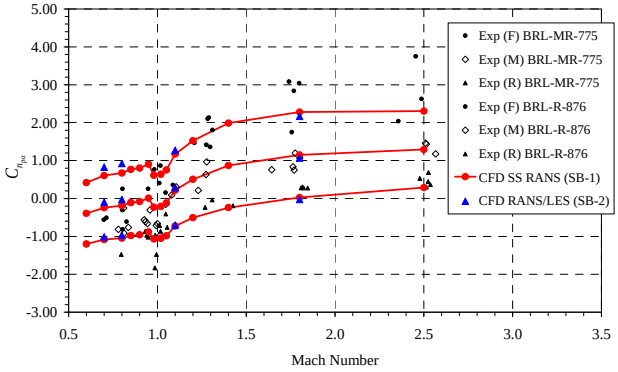

Figure 5. Comparison of predicted and experimental Magnus moment at (a) $\alpha = 2°$ for and (b) $\alpha = 5°$ for ANSR.

After observing these Magnus moment trends in the M910 and the 0.50-cal. projectiles, another study was performed using the ANSR (DeSpirito, 2008a), as a large amount of archival experimental data exists (Schmidt and Murphy, 1954; Murphy and Schmidt, 1953; Nielsen and Platou, 1974). The ANSR configuration has a sharp edge at the base (both with and without boattail), similar to that in an earlier small caliber munitions study (Weinacht, 2007). It was desired to see if the sharp-edge-base projectile would lead to more accurate Magnus moment predictions using steady-state CFD. Figure 5 shows the comparison of the experimental and predicted Magnus moment for the ANSR for three different c.g. locations. There is little difference between the Magnus moment predicted via the RANS and RANS/LES simulations, regardless of Mach number or c.g. location. There is excellent agreement between the predicted and experimental Magnus moment from about Mach 0.98 and above. Although the Magnus moment is again over predicted in the subsonic range, the differences are not as great as for the M910 or 0.50-cal. projectiles. Similar agreement was found for a 0.5-cal., 7° boattail version of

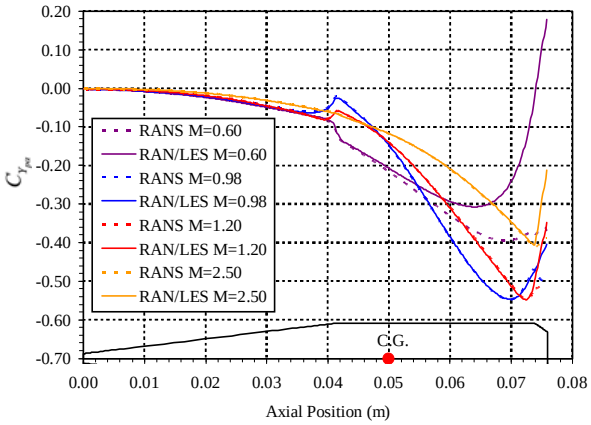

(a)

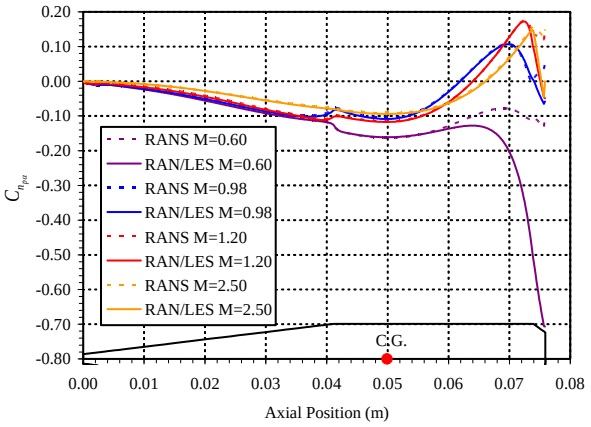

(b)

Figure 6. Distributions of Magnus force and moment along M910 projectile body: Magnus (a) force and (b) moment at $\alpha = 3°$; (c) angle of attack effect on RANS/LES Magnus moment predictions.

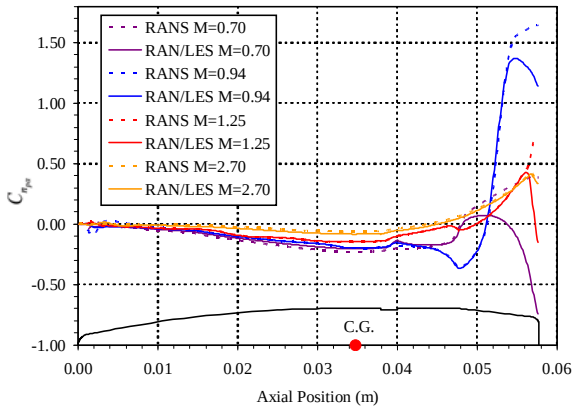

Figure 7. Distribution of Magnus moment along 0.50-cal. projectile body ($\alpha = 2°$).

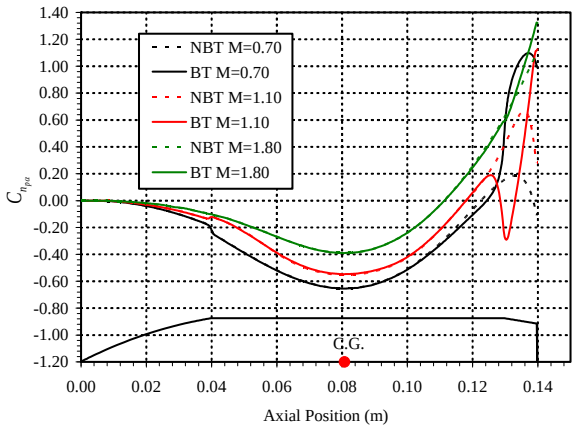

Figure 8. Distribution of Magnus moment along ANSR projectile body ($\alpha = 2°$).

the ANSR, also with a sharp corner at the base (DeSpirito, 2008a). This result indicates that a sharp-edge-base projectile may inhibit the impact of the unsteady flow phenomena on the accuracy of steady-state RANS simulations.

Evaluations of force and moment distributions along the projectile length clearly show that the effects on Magnus are confined to the rear end of the projectile (Figure 6). The differences between the RANS and RANS/LES simulations are confined to the chamfer region and are not too large for the transonic and supersonic Mach numbers. However, at Mach 0.6, the RANS/LES Magnus force and moment distribution predictions begin to differ from the RANS predictions a significant distance forward on the body, with the final magnitudes much different between the two.

The Magnus force (Figure 6a) is typically negative along the body (i.e., normal pointing to port side of projectile for right-hand spin). At Mach 0.6, the total Magnus force goes positive, indicating that unsteady flow interactions have overtaken the true "Magnus" effects. For example, for most of the Mach numbers, the side (Magnus) force center of pressure in the RANS/LES simulations is forward of the c.g., with the negative Magnus force generating a negative (nose left) Magnus moment. At Mach 0.6, the side force is positive, so the negative Magnus moment indicates the center of pressure has moved rearward of the c.g.

Similar distributions are observed for the 0.50-cal. projectile, Figure 7. At Mach 2.7 there is virtually no difference between the RANS and RANS/LES Magnus moment distributions. As the Mach number decreases, the total difference between each type of simulation tends to increase and the distributions diverge further forward on the body. Figure 8 shows the difference between the Magnus moment distributions for the square-base (NBT) and boattail (BT) ANSR configurations. The boattail leads to increased Magnus moment, especially at subsonic and transonic Mach numbers. For the ANSR, there were

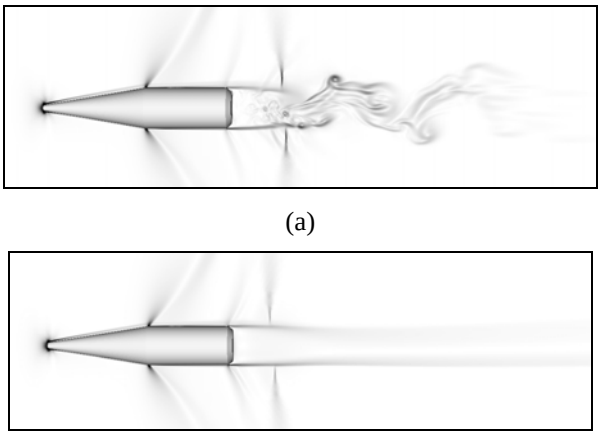

(a)

(b)

Figure 9. Numerical Schlieren of the M910 flow field: (a) instantaneous RANS/LES and (b) RANS simulation at Mach 0.98, $\alpha = 3°$.

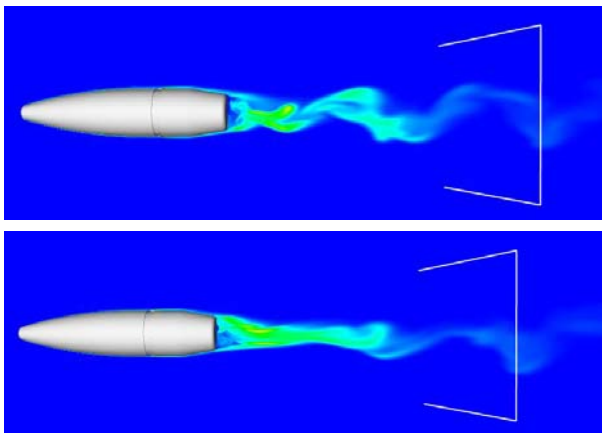

Figure 10. Instantaneous turbulent kinetic energy, 0.50-cal. projectile, at (top) Mach 0.70 and (bottom) Mach 1.25 and $\alpha = 2°$.

only minor differences between the Magnus moment distributions predicted from the two simulation methods. The sharp edge at the base of the ANSR (both square-base and boattail configurations) leads to a well-defined separation point, which may be a possible reason the steady-state RANS simulations can better predict the Magnus effects. The chamfer on the M910 and the rounded base of the 0.50-cal. projectile are likely responsible for requiring the time-accurate RANS/LES simulations.

It is believed that at lower Mach numbers, the unsteady wake flow interacts with the asymmetric pressure distribution (which is responsible for the Magnus effect) on the projectile body. This interaction effect is not always captured by the steady-state simulations. The wake effects on the body forces are likely small enough not to significantly impact the normal force and pitching moment; however, the Magnus effects are much smaller and the small wake effect perturbations may significantly effect the Magnus moment. Figure 9 illustrates the differences between the flow field obtained using the time-accurate RANS/LES (the LES mesh region extends about 1 body length downstream of projectile) and the steady-state RANS simulations at Mach 0.98. At higher Mach numbers, the flow fields calculated by the two methods begin to look similar. However, at lower, especially subsonic, Mach numbers, the unsteady eddies in the wake were resolved when RANS/LES is used (Figure 10). The outlines in Figure 10 mark the extent of the LES mesh; after this region, the turbulent eddies will be dissipated due to mesh stretching.

Results from these studies indicate that the projectile base shape plays a role in both the level of Magnus nonlinearity and the accuracy of the prediction from the steady-state CFD simulation compared to that from the RANS/LES simulation. Another study was recently performed (DeSpirito, 2008b) to investigate these effects in a controlled manner. The 5-cal. version of the ANSR (Murphy and Schmidt, 1953; Nielsen and Platou, 1974) was used as the reference projectile, as this body length is similar to most medium and large caliber munitions. CFD was used to characterize the aerodynamics of five projectile configurations. These included the standard no-boattail (NBT) and 0.5-cal, 7° boattail (BT) configurations investigated in the archival references. Three additional configurations were generated by putting new base shapes on the ANSR forebody: a 0.123 cal. chamfer (CHM) similar to the M910 projectile base; a 0.78 cal., 9° radius boattail (50CBT) similar to the standard 0.50-cal. projectile base; and a hemispherical base (HEMI). The hemispherical base is usually avoided due to problems with dynamic stability and was chosen to illustrate that Magnus effects contribute to these problems.

Figure 11 shows turbulent kinetic energy contours for each of the five configurations. The plots are from one time step of the time-accurate RANS/LES simulations, giving an instantaneous picture of the flow field. Plots from the steady-state RANS simulations (not shown) give an "averaged" picture of the flow field and do not show the turbulent eddy structures (DeSpirito, 2008b). The time-averaged flow field of the RANS/LES simulations, from which the coefficients were calculated, resembles the RANS flow field. Subtle differences in the wake flow can be observed. The boattail (Fig. 11b,d) causes a thickening of the boundary layer along the boattail and a narrowing of the wake due to the boattail angle. The chamfer (Fig. 11c) causes some narrowing of the wake, but not as much as the boattail. The effect of the hemispherical base (Fig. 11e) on the wake is in between that of the square base and the boattail configurations. The highest level of turbulent kinetic energy is found for the NBT and CHM configurations.

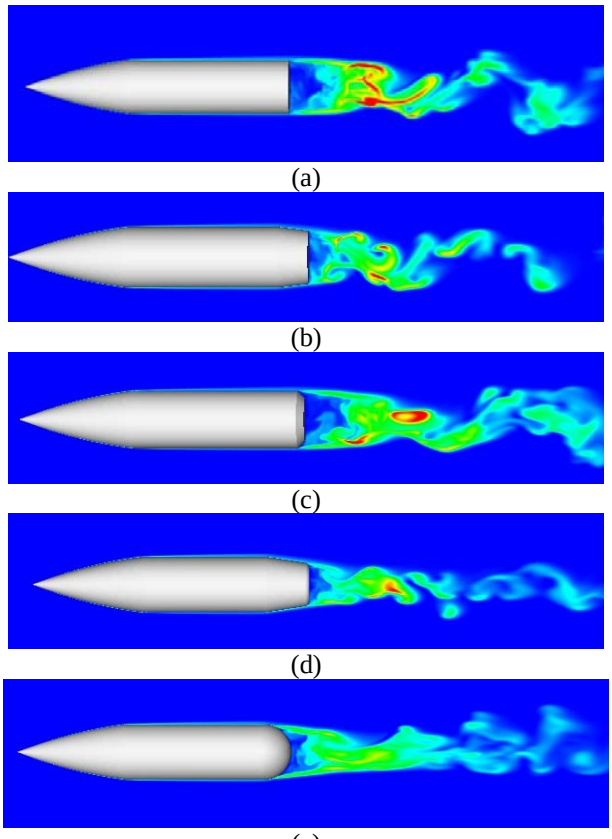

Figure 11. Instantaneous RANS/LES turbulent kinetic energy contours at Mach 0.7 and $\alpha = 2°$: (a) NBT, (b) BT, (c) CHM, (d) 50CBT, and (e) HEMI configurations (contour range: 0–2000 for all plots).

Figure 12 shows the Magnus moment coefficient predictions for the 5 base configurations. Reasonably good agreement is observed between the predicted and experimental data (Murphy and Schmidt, 1953; Nielsen and Platou, 1974) for the NBT and BT configurations. The CHM configuration shows a small decrease in the linear Magnus moment coefficient over that of the NBT configuration fairly consistent across the Mach number range. The presence of a boattail causes an increase in the Magnus moment in the subsonic and transonic flight regimes that continues to increase with boattail length. The Magnus moment in the supersonic flow is unchanged by adding a boattail. The HEMI configuration shows a significantly different effect on the linear Magnus moment, which decreases across the Mach number range. The effect is especially strong in the transonic region, $0.7 < M < 0.98$, where a significant drop in Magnus moment is observed. The change in Magnus moment in the transonic regime is important to the dynamic stability of a round (McCoy, 1998), especially for artillery projectiles, as a large portion of their flight is in this Mach number regime. The Magnus moment characteristics of

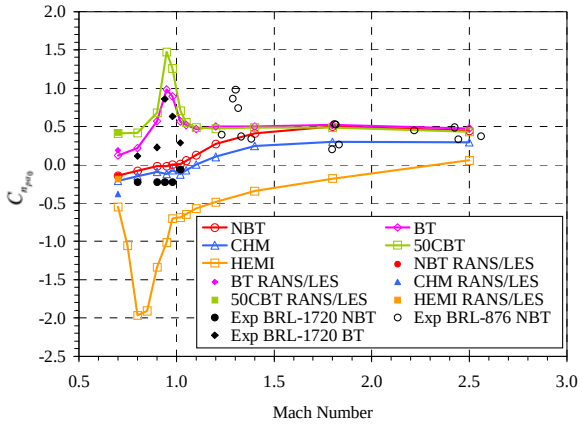

Figure 12. Linear Magnus moment coefficients vs. Mach number.

the HEMI configuration would likely lead to stability issues in the transonic flight range.

There was very little difference between the Magnus moments predicted using the RANS or RANS/LES methods for the NBT, BT, and 50CBT configurations at Mach 0.7. This is consistent with a previous study investigating the Magnus characteristics of the 7-cal. ANSR (DeSpirito, 2008a). The RANS/LES predictions for the CHM configuration showed a lower Magnus moment, which is also consistent with previous studies on the Magnus characteristics of the M910 projectile (DeSpirito and Heavey, 2004; DeSpirito and Plostins, 2007). In the M910 studies, the lower Magnus moments predicted using the RANS/LES simulations improved the CFD prediction compared to experimental flight data. The RANS/LES prediction of Magnus moment for the HEMI configuration showed an increase over the RANS configuration. Although no experimental data is available for this configuration, it is likely that the RANS/LES prediction is an improvement over the RANS prediction since the time-accurate calculation will more accurately simulate the wake flow that affects the forces on the rear of the projectile.

The cubic Magnus moment coefficients were also calculated and the HEMI configuration showed the largest nonlinear component. The largest difference between the steady-state and RANS/LES prediction of cubic Magnus moment was for the 50CBT and HEMI configurations, which have rounded bases. This result confirms the observation of Weinacht (2007) that a rounded base is more susceptible to nonlinear Magnus effects.

4. SUMMARY

Time-accurate RANS/LES simulations were found to improve the Magnus moment prediction for projectiles with rounded or chamfered bases. No difference was found between the steady-state and time-accurate

simulations for the projectile with a sharp-cornered base—either with or without a boattail. Flow field visualizations showed that the near-body flow field is similar for steady-state RANS and time-accurate RANS/LES simulations. However, the RANS/LES simulations resolved the turbulent eddies shed from the projectile base. Magnus effects were found to be concentrated near the base of the projectile. Boattail and hemispherical base configurations showed the largest effect on Magnus moment. Further study is planned to investigate the physical phenomena responsible for the observed effects.

The computation of projectile aerodynamics using time-accurate RANS/LES methods is a relatively new approach. Although computationally more expensive than traditional RANS approaches, the RANS/LES method is likely the only computationally efficient way to predict aerodynamic coefficients that are impacted by highly separated flow phenomena, such as Magnus effects and high angle of attack flight scenarios. Validating this advanced method and adding it to the Army's computational toolbox will advance the state-of-the-art and enable prediction of highly maneuverable, precision munition systems.

ACKNOWLEDGEMENTS

The authors thank Dr. Paul Weinacht, ARL, for many helpful discussions. This work was supported in part by a grant of high-performance computing time from the U.S. Dept. of Defense High Performance Computing Modernization program at the ARL MSRC, Aberdeen Proving Ground, Maryland.

REFERENCES

DeSpirito, J., "CFD Prediction of Magnus Effect in Subsonic to Supersonic Flight," AIAA-2008-0427, Jan. 2008a.

DeSpirito, J., "Effects of Base Shape on Spin-Stabilized Projectile Aerodynamics," AIAA-2008-6738, Aug. 2008b.

DeSpirito, J., and Heavey, K. R., "CFD Computation of Magnus Moment and Roll Damping Moment of a Spinning Projectile," AIAA-2004-4713, Aug. 2004.

DeSpirito, J., and Plostins, P., "CFD Prediction of M910 Projectile Aerodynamics: Unsteady Wake Effect on Magnus Moment," AIAA-2007-6580, Aug. 2007.

DeSpirito, J., Silton, S. I., Weinacht, P., "Navier-Stokes Predictions of Dynamic Stability Derivatives: Evaluation of Steady-State Methods," AIAA-2008-0214, Jan. 2008.

McCoy, R. L., Modern Exterior Ballistics: The Launch and Flight Dynamics of Symmetric Projectiles. Schiffer Books, Atglen, PA, 1998, pp. 273–298.

Murphy, C. H. and Schmidt, L. E., "The Effect of Length on the Aerodynamic Characteristics of Bodies of Revolution in Supersonic Flight," U.S. Army Ballistics Research Laboratory, BRL-R-876, Aberdeen Proving Ground, MD, August 1953.

Nielsen, G. I. T., and Platou, A. S., "The Effect of Conical Boattails on the Magnus Characteristics of Projectiles at Subsonic and Transonic Speeds," U.S. Army Ballistics Research Laboratory, BRL-R-1720, Aberdeen Proving Ground, MD, June 1974.

Nietubicz, C. J., Sturek, W. B., and Heavey, K. R., "Computations of Projectile Magnus Effect at Transonic Velocities," U.S. Army Ballistic Research Laboratory, BRL-TR-02515, Aberdeen Proving Ground, MD, Aug. 1983.

Plostins, P., McCoy, R. L., and Wagoner, B. A., "Aeroballistic Performance of the 25mm M910 TPDS-T Range Limited Training Projectile," U.S. Army Ballistics Research Laboratory, BRL-MR-3886, Aberdeen Proving Ground, MD, Jan. 1991.

Sahu, J., "Transonic Navier-Stokes Computations for a Spinning Body of Revolution," U.S. Army Ballistic Research Laboratory, BRL-TR-3265, Aberdeen Proving Ground, MD, Sep. 1991.

Schmidt, L. E., and Murphy, C. H., "The Aerodynamic Properties of the 7-Caliber Army-Navy Spinner Rocket in Transonic Flight," U.S. Army Ballistics Research Laboratory, BRL-MR-775, Aberdeen Proving Ground, MD, March 1954.

Silton, S. I., "Navier-Stokes Computations for a Spinning Projectile from Subsonic to Supersonic Speeds," *J. of Spacecraft and Rockets*, Vol. 42, No. 2, 2005, pp. 223–231.

Silton, S. I., "Navier-Stokes Predictions of Aerodynamic Coefficients and Dynamic Derivatives of the 0.50-cal. Projectile," *47th AIAA Aerospace Sciences Meeting*, Orlando, FL, Jan. 2009.

Simon, F., Deck, S., Guillen, P., and Sagaut, P., "Reynolds-Averaged Navier-Stokes/Large-Eddy Simulations of Supersonic Base Flow," *AIAA Journal*, Vol. 44, No. 11, 2006, pp. 2578–2590.

Simon, F., Deck, S., Guillen, P., Cayzac, R., and Merlen, A., "Zonal-Detached-Eddy Simulation of Projectiles in the Subsonic and Transonic Regimes," *AIAA Journal*, Vol. 45, No. 7, 2007a, 1606–1619.

Simon, F., Deck, S., Guillen, P., Cayzac, R., Sagaut, P., and Merlen, A., "RANS/LES Simulations of Projectiles With and Without Rotation in the Subsonic and Transonic Regimes," *Proceedings of the 23rd International Symposium on Ballistics*, Tarragona, Spain, Apr. 2007b.

Sturek, W. B., and Schiff, L. B., "Computations of the Magnus Effect for Slender Bodies in Supersonic Flow," *AIAA Journal*, Vol. 20, No. 12, 1982, pp. 1724–1731.

Weinacht, P., "Characterization of Small-Caliber Ammunition Performance Using a Virtual Wind Tunnel Approach," AIAA-2007-6579, Aug. 2007.

Weinacht, P., and Sturek, W. B., "Navier-Stokes Predictions of Pitch Damping of Finned Projectiles Using Steady Coning Motion," AIAA-90-3088, Aug. 1990.

Weinacht, P., Sturek, W. B., and Schiff, L. B., "Navier-Stokes Predictions of Pitch Damping for Axisymmetric Projectiles," *J. of Spacecraft and Rockets*, Vol. 34, No. 6, 1997, pp. 753–761.